Polymer 312 (2024) 127644

Contents lists available at ScienceDirect

Polymer

journal homepage: www.elsevier.com/locate/polymer

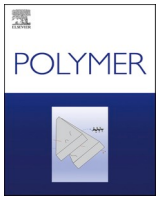

Effect of polymer-entwined reduced graphene oxide laminates on the performance and stability of forward osmosis membranes for water desalination

Mohamed Edokali [a,*], Rachel Bocking [b], Alexander Massey [b], Abdulhakim Al Hinai [a], David Harbottle [a], Robert Menzel [b], Ali Hassanpour [a]

[a] School of Chemical and Process Engineering, Faculty of Engineering and Physical Science, University of Leeds, Leeds, LS2 9JT, UK
[b] School of Chemistry, Faculty of Engineering and Physical Science, University of Leeds, Leeds, LS2 9JT, UK

ARTICLE INFO

Keywords:
Forward osmosis membranes
Reduced graphene oxide
Hyperbranched polyethylenimine
Polyethylene glycol
Water desalination
Membrane stability

ABSTRACT

Layered graphene oxide (GO) membranes have been widely employed for water desalination in forward osmosis (FO) systems, however, the balance between performance and long-term stability of membranes is still a trade-off in the practical application. A newly developed laminar GO-based FO membrane was prepared by a two-step protocol, including acid treatment of GO before crosslinking and reduction of GO by hyperbranched polyethylenimine (HPEI), and followed by coating HPEI-reduced graphene oxide (HPEI:rGO) laminates by polyethylene glycol (PEG). It is suggested that the long-chain and amino-enrichment HPEI polymer can be covalently bonded with the acid-treated GO at elevated temperatures. This chemical process partially removed oxygen-containing functional groups of GO and formed a nanocomposite structure with tuned interlaminar spacing for better selectivity of NaCl ions. Subsequently, the infiltration of PEG molecules through the HPEI-rGO structure improved the hydrophilicity, and hence the water permeability across the PEI60k:rGO/PEG membrane. In this study, the resultant membrane exhibited water flux of 7.7 LMH, salt rejection efficiency of 97.9 %, and low reverse solute flux of 0.56 gMH in an FO filtration process. Also, synergistic effects of the double-polymer modification reinforced enhancement of dimensional integrity and durability of the membrane structure in both ionic and harsh conditions.

ABBREVIATIONS

AFM	Atomic force microscopy	ICP	Internal concentration polarisation
C/O	Carbon-to-oxygen ratio	LBL	Layer-By-Layer
$C_6H_{12}O_6$	Dextrose	LMH	Litres per square meter per hour
CA	Cellulose acetate	N_2	Nitrogen
CHNS–O	Carbon, hydrogen, nitrogen, sulfur, and oxygen analyser	NaCl	Sodium chloride
CTA	Cellulose Triacetate	PEG	Polyethylene glycol
DIW	Deionised water	PEI60k: rGO	Polyethylenimine functionalised reduced graphene oxide
DLS	Dynamic light scattering	PEI60k: rGO/PEG	Polyethylenimine functionalised- polyethylene glycol reduced graphene oxide
EDX	Energy dispersive X-ray spectroscopy	R_a	Average surface roughness
EPD	Electrophoretic deposition	rGO	Reduced graphene oxide
FE-SEM	Field emission scanning electron microscopy	R_{max}	Maximum roughness depth roughness
FO	Forward osmosis	RO	Reverse osmosis
FTIR	Fourier transform infrared Spectroscopy	rpm	Revolutions per minute
gMH	Grams per square meter per hour	R_q	Root-mean-squared roughness
GO	Graphene oxide	RSF	Revere solute flux
HCl	Hydrochloric acid	WCA	Water contact angle
HD	Hydrodynamic size diameter	XRD	X-ray diffractometer

(*continued on next column*)

(*continued*)

(*continued on next page*)

* Corresponding author.
E-mail addresses: M.S.Edokali@leeds.ac.uk, edokali@yahoo.co.uk (M. Edokali).

https://doi.org/10.1016/j.polymer.2024.127644
Received 31 July 2024; Received in revised form 17 September 2024; Accepted 19 September 2024
Available online 21 September 2024

(*continued*)

HPEI	Hyperbranched polyethylenimine	ZP	Zeta potential

1. Introduction

Water crisis is becoming inevitably problematic to humankind due to the limited resources of freshwater on the earth [1,2]. Researchers have recently given an intensive attention to develop various water treatment technologies to meet the global demand for clean water access [3]. As such, forward osmosis (FO) has been considered as one of the efficiently innovative water treatment and purification processes owing to its lower energy consumption compared to the reverse osmosis (RO) [4,5]. FO is osmotically driven technique by the natural pressure generated from the difference in concentrations between feed and draw solutions across a semipermeable membrane for water desalination [6,7]. However, there are still challenges with FO prior to its practical implementation for water desalination, including low water permeability, internal concentration polarisation (ICP) and reversible membrane fouling, efficient solutions to tackle these key concerns in FO processes remain needed [4]. These issues are mainly related to few types of commercially-available polymeric membranes which provide limited and insufficient water flux [8]. Therefore, there has been recently an emerging need to develop alternative membranes for commercially-available FO polymeric membranes which can improve the performance of FO desalination [9].

In recent years, graphene, and its derivatives (e.g., especially graphene oxide (GO)) have been considered as an excellent candidate for the fabrication of water-based desalination membranes [10–15]. This is attributed to their unique two-dimensional laminar structure, high hydrophilicity, and abundantly oxygen functional groups [13,15]. Several studies have been devoted to developing the implementation of GO sheets as a selective layer for FO desalination films using several approaches such as vacuum-assisted filtration, spin-coating, drop-casting, layer-by-layer (LBL) [16], and recently electrophoretic deposition (EPD) [17]. However, the stability of pristine GO membranes in wet environments remain the bottleneck for their practical implementation due to the weak hydrogen bonds between oxygen functional groups of GO sheets [18]. This can lead to enlarge the interlayer spacing between GO sheets, and thus significantly expand the nano-channels in the membrane [19–21]. As such, this can lower the rejection performance towards small ionic species than common FO membranes. Moreover, the chemical and mechanical stability of GO-based laminar FO membranes is still challenging since the practical application of FO desalination involves physical and chemical washing procedures [22–24]. Therefore, there is an urgent need to develop the design criteria and assembling processes of GO-based membranes to overcome the trade-off between chemical and physical stability and desalination performance in FO processes [24].

Recently, there has been reported that several strategies are being developed to overcome the stability issues of GO membranes in FO desalination [24,25]. GO laminates in FO membranes can be improved by chemically reducing their oxygen-containing functional groups, crosslinking with different chemical agents and nanoparticles, or a combination of both [17,19,21,23,26–31]. In addition, Other GO-based membrane fabrication strategies involved the reduction of GO laminates, and this can be followed by infiltration of charged nanomaterials [i.e., polydopamine (pDA) and polystyrene sulfonic acid (PSS)] [16,32]. Consequently, the stability of GO layers can be enhanced, and the nanochannels can relatively be tuned, which can increase the rejection performance towards hydrated salt ions [33]. Nevertheless, water transport across modified GO membranes could be obstructive by an uncontrolled reduction of GO laminates or addition of different agents, which might lead to altering GO nanochannels or formation of more compact structure of GO membranes [28]. Therefore, there is still an urgent demand to search for more effective cross-linkers that can facilitate the fabrication of promising GO-FO membranes which is yet not to be achieved.

In this regard, it has been reported in the literature that hyperbranched polyethylenimine (HPEI) was remarkably successful in enhancing GO membranes' hydrophilicity and rejection efficiency towards heavy metal and ionic species through functionalisation with amine groups [18,34]. This can be achieved by combination strategies of Donnan effects and size exclusion for ions separation mechanisms [34]. However, long-term stability of HPEI-GO membranes remain not known in FO desalination. As such, polyethylene glycol (PEG), as a non-toxic polymer and biocompatible agent, has been extensively functionalised and studied in several applications to enhance the surface modification and stability of GO sheets *via* covalent and non-covalent processes [35–38]. Previous studies have importantly demonstrated that the cross-linking approach of GO-based membranes specifically relies on the functionalisation of GO sheets [18,34].

In this work, a novel two-step modification strategy is designed and employed to prepare highly stable and charged GO-based FO membranes. The protocol mainly includes **(i)** crosslinking, reduction, and amine-enrichment modification of Hydrochloric acid (HCl)-treated GO sheets by HPEI, and **(ii)** infiltration of water dispersible PEG through the microstructure of HPEI-functionalised reduced graphene oxide (rGO) film to enhance its wettability and stability. The activation and stabilisation of carbon groups of GO sheets is the key factor for construction of sufficiently active site anchors for reaction with amine groups from HPEI and PEG. For this purpose, the GO was initially treated with HCl acid, and subsequently reduced and crosslinked with HPEI, followed by the deposition of HPEI-rGO dispersion on a polymer substrate *via* a vacuum-assisted assembly technique, while the ultimate step was to increase the hydrophilicity and provide a high dimensional stability of the as-prepared membrane by the infiltration of PEG. To best of our knowledge, this is the first time to report the two-step functionalisation approach to bind GO with HPEI and PEG for fabrication of a stable FO-based desalination membrane. The novelty of this work lies in the development of the above protocol for laminated HPEI/PEG-modified rGO membranes. Key innovative aspects include: **(1)** *Enhanced functionalisation stability:* HCl treatment of GO to improve chemical stability and reactivity, preventing degradation during high-temperature wet-chemical processes. (2) *Optimised cross-linking:* Controlled cross-linking of HPEI with HCl-treated GO and subsequent PEG modification, resulting in stable and laminated rGO membranes. (3) *Improved membrane performance:* Optimisation of HPEI and PEG incorporation conditions, producing membranes with improved properties, as evidenced by detailed characterisations. This method addresses significant challenges in GO functionalisation and stability, advancing membrane materials for desalination applications. The functionalisation approach of GO, and crosslinking and modification of GO membranes were discussed in more detail. The optimisation process for selecting the most stable HPEI-rGO dispersion for preparation of membranes was also further studied. Different characterisations, including physicochemical and morphological properties, were conducted to investigate and evaluate the surface properties and stability performance of rGO modified membranes. In addition, the desalination performance of crosslinked membranes was evaluated in FO laboratory-scale process. This study could remarkably provide the breakthrough for design and fabrication of new generations of promising FO membranes.

2. Experimental

2.1. Chemicals and materials

Freeze-dried GO powder (*with a variable particle size*) was obtained from William Blythe, UK. Hydrochloric acid (0.1 M) was purchased from Fisher Scientific, UK. Hyperbranched Poly (ethylenimine) solution

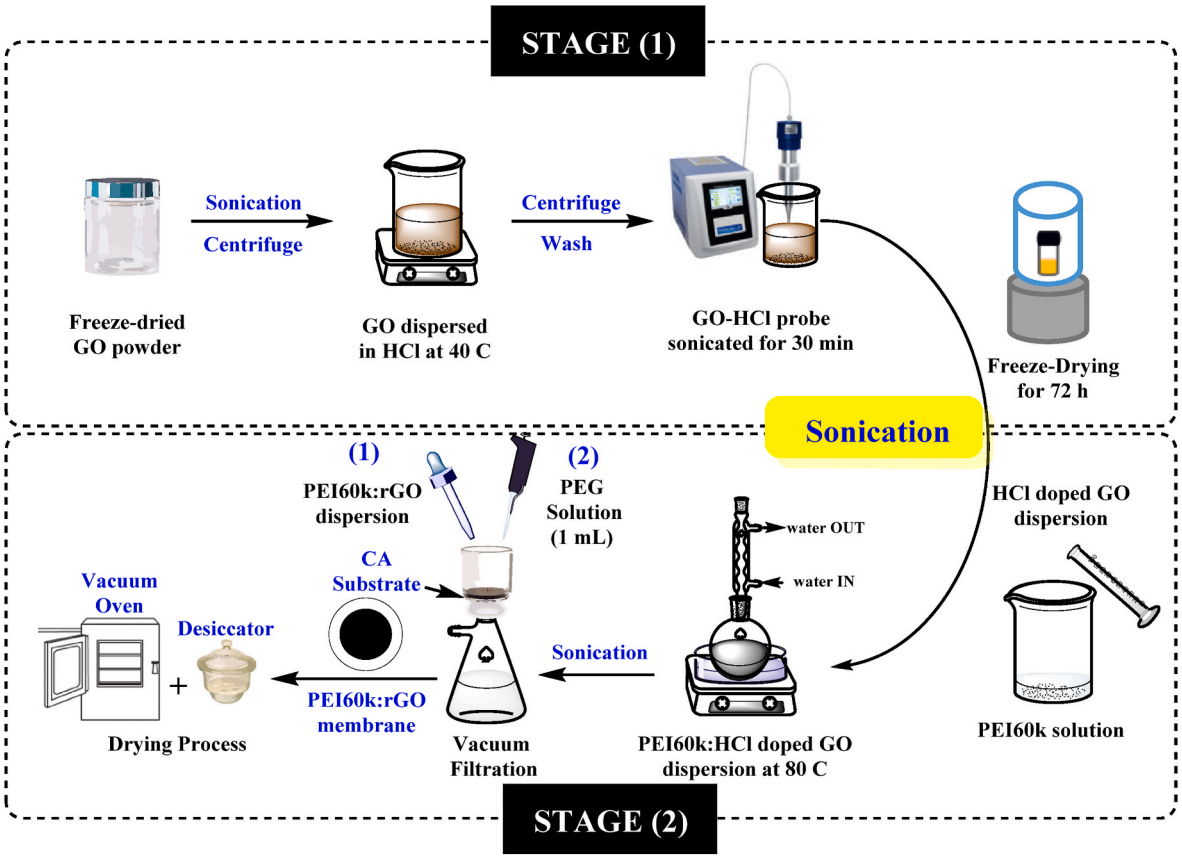

Scheme 1. Diagram of functionalisation procedures of acid-treated GO, and preparation of modified rGO membranes.

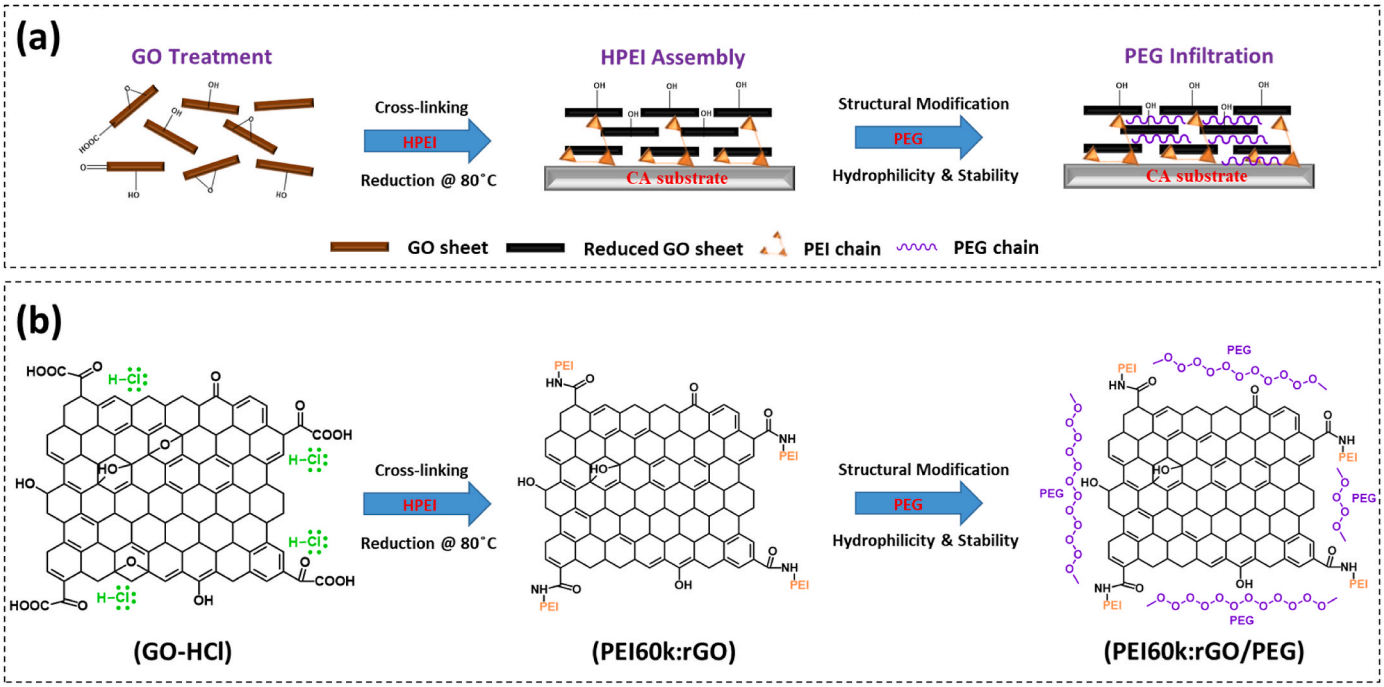

Fig. 1. **(a)** Schematic of the synthesis process, and **(b)** associated mechanisms of laminated GO and PEI60k:rGO frameworks, and the fabrication method of PEI60k:rGO/PEG membranes.

(HPEI, M_n: 60,000 – M_w: 750,000 g/mol, 50 wt % in H_2O) and Polyethylene glycol (PEG, $(C_2H_4)_n.H_2O$, M_w: 10,000 g/mol) were purchased from Sigma-Aldrich, UK. Commercial FTSH2O Cellulose Triacetate flat sheet membrane (CTA with an averaged pore size: ~0.45 μm, porosity: ~70 %, thickness: ~50 μm [39–41]) was purchased from STERLITECH, U.S. Commercial Cellulose Acetate (CA) membrane filters (pore size:

0.22 μm, porosity: 80 %, diameter: 47 mm) were obtained from CamLab, UK. Sodium chloride (NaCl, M_w: 58.44 g/mol) was purchased from VWR, UK. Dextrose ($C_6H_{12}O_6$, M_w: 180.16 g/mol) was purchased from Alfa Aesar, UK. Deionised water (DIW), with a resistivity of 18.2 mΩ-cm at 25 °C, was collected from an ultrapure water purification system and used throughout this study. All chemicals and reagents were of analytical grade purity and used as received.

2.2. Methods

The facile preparation protocol of laminated HPEI/PEG-modified rGO membranes was developed, as illustrated in Fig. (1) (see Scheme 1). The targeted protocol was simply divided into two main stages as follows:

2.2.1. STAGE (1): preparation of HCl-treated GO sheets

Our initial synthetic efforts to functionalise GO sheets with HPEI were unsuccessful, showing minimal or no reactivity between GO and HPEI. Literature work has shown that GO can easily degrade during wet-chemical functionalisation procedures at increased temperatures. Therefore, GO was treated with HCl prior to HPEI functionalisation, following a literature procedure that has shown substantially improved chemical GO stability and reactivity upon HCl treatment [42]. Briefly, freeze-dried GO powder (200 mg) was dispersed in 200 mL of DIW and sonicated using a probe sonicator (Fisher Scientific FB705-700w ultrasonic homogenizer), with an amplitude of (50) and power of 40 W, for 30 min to get a homogeneous GO solution. The obtained GO dispersion was then centrifuged (ThermoFisher Scientific, Megafuge™ R16 Centrifuge Series) at 10,000 rpm for 30 min to remove the supernatant which contained minor amounts of few layered GO. GO particles were further washed three times by DIW using a centrifugation process at 10, 000 rpm for 1 h. The obtained GO was then dispersed in 0.5 mL of hydrochloric acid (0.1 M) and stirred (Asynt, ADS-HP-NT hotplate stirrer) for about 30 min at 40 °C in a water bath. The HCl-treated GO was further washed eight times by DIW using a centrifuge (10,000 rpm, 1 h) until the pH (Mettler Toledo SevenCompact S220 pH meter) of the supernatant reached neutral to remove excess of acid. Finally, the final product was freeze-dried (LABCONCO FreeZone −50 °C Benchtop Freeze Dryer) for 72 h to yield brown/green particles which were stored in a desiccator under N_2 gas. **Scheme (1)** also shows adapted steps of functionalising GO with HCl in the first stage of the chemical synthesis.

2.2.2. STAGE (2): facile preparation of cross-linked and modified rGO membranes

A certain amount of freeze-dried HCl-treated GO (50 mg) was dispersed in 50 mL of DIW by ultra-sonication (BRANSONIC 2800-E CPX ultrasonic water bath) for 30 min to produce HCl-GO dispersion (1 mg/mL). The resultant dispersion and controlled amount of HPEI solution were mixed, by adding HCl-GO dropwise into the HPEI solution to avoid any aggregations, under a vigorous stirring, and subsequently ultra-sonicated further for 10 min in a water bath. The mixture was refluxed under a vigorous stirring at 80 °C for 2 h. At this stage, a further reaction was occurred at which the brown/green coloured HCl-GO dispersion turned to be darker black coloured which elucidated the transformation of GO to rGO. Different HPEI-GO feeding ratios (0.01:1, 0.06:1, 0.1:1 and 1:1) were considered and compared during the fabrication process. After optimising the most stable feeding concentration of 0.06 mg/mL **(**see **Section S1, SI)**, the obtained homogenous dispersion was vacuum filtrated through the CA support filter membrane, and self-assembly of HPEI-rGO laminates occurred during the filtration process (*denoted as PEI60k:rGO*). Subsequently, a controlled amount (1 mL) of the as-prepared PEG solution (*with an optimised concentration of 0.*1 mg/mL **(**see **Section S2, SI)**) was also vacuum filtered through the PEI60k:rGO film, followed by rinsing with DIW to remove the excess of PEG (*denoted as PEI60k:rGO/PEG*). The resultant membranes were then kept in a desiccator for 24 h before drying in a vacuum oven (GALLENKAMP Fistreem vacuum oven) at 40 °C for 2.5 h. Lastly, the obtained membranes were again stored in a desiccator for further use. For characterisation comparison, HCl-treated GO dispersion (1 mg/mL) was also vacuum filtered through the commercial CA substrate and similarly dried to form a control sample (*denoted as GO*). The schematic illustration by which the preparation of the crosslinked rGO membranes was indicated in the second stage of the membrane fabrication process, as presented in **Scheme (1)**.

As shown in Fig. (S3), the HCl-treated GO membrane (GO membrane) demonstrated a dark, brown/green colour owing to the reduction of natively hydroxyl groups present in GO during the esterification process [21,42]. Contrastingly, as-prepared PEI60k:rGO and PEI60k: rGO/PEG membranes exhibited graphitic-like black surfaces. This is attributed to recovery of graphitic sp^2 bonding and reduction of oxygen-containing functional groups [43].

2.3. Material and membrane characterisation

Physicochemical properties and morphologies of the as-prepared dispersions and membranes were characterised using various analytical techniques. The hydrodynamic size diameter (HD) and surface charges were together measured by the dynamic light scattering (DLS, with dual-angle measurements) using Zeta potential (ZP) analyser (Malvern Zetasizer Nano ZSP ZEN5600). The percentage of elemental chemical compositions was determined using the CHNS–O analyser (Flash EA2000 elemental analyser, ThermoFisher Scientific). The interlayer spacing (i.e., nanochannels) between modified GO and rGO membranes was analysed using X-ray diffraction (XRD, Bruker D8 advance diffractometer equipped with K-Cuα and radiation 1.5406 Å) with 2 θ range from 5° to 50° and scanning rate range between 0.25°/min and 1°/min. In addition, the XRD data was processed as follows: **(i)** baseline was subtracted, **(ii)** scale was normalised, and **(iii)** cosmic rays and peak noises were removed. Chemical functionality of membranes were characterised using Fourier transform infrared spectrometer (FTIR, Nicolet iS10, ThermoFisher Scientific) in the range from 525 to 4000 cm^{-1} with a scanning resolution of 16 cm^{-1}. Surface morphology, microstructure and surface chemical compositions of membranes were characterised by field emission scanning electron microscope (FE-SEM, Hitachi SU8230, Leeds Electron Microscopy and Spectroscopy Centre) operated at 2 kV and equipped with an energy-dispersive X-ray (EDX, Oxford Aztec INCA 350) spectroscopy. The Surface topography of membranes, in terms of root-mean-squared (R_q) surface roughness, average surface roughness (R_a) and maximum roughness depth (R_{max}), was investigated under non-contact mode and over a scanning area of [1.0] x [1.0] μm^2 by atomic force microscopy (AFM) using (Bruker Innova-IRIS AFM system). The surface wettability of membranes was determined by measuring water contact angle (WCA) of DIW droplets on the surface of membranes at 25 °C using the sessile drop method (SMaRT, KSV CAM 200 Optical Contact Angle Tensiometer).

2.4. Evaluation of membrane performance in an FO process

The performance of membranes was conducted in a laboratory-scale FO system for 2 h, as shown in Fig. S4 (a) and **(b)**. The system contains of an in-house designed and built membrane cell (with an active membrane area of 6.16 cm^2), as depicted in Fig. S5, which was set up in FO mode (*i.e., the active layer of membrane facing the feed solution tank and the* support *layer facing draw solution tank*). The feed solution tank was filled with 1 L of DIW, whereas the draw solution tank was filled with 1 L of 0.6 M NaCl ionic solution. Before commencing the FO tests, concentrations of the feed and draw solutions were individually assessed and recorded. This ensured that any variations in the ionic contents of the feed solution during FO operations were solely due to the reversed NaCl ions. This was achieved by calculating the difference between the concentration of the DS (comprising NaCl solution) at specific time intervals and the initial concentration of DIW as FS at the starting time (0 min). The feed and

draw solution were set to be continuously circulated counter-currently across the membrane at room temperature with a constant flowrate of 200 mL/min (~2.3 cm/s and 0.5 bar) using two gear pumps (Model: 07555-15, Masterflex™, Cole-Parmer™, U.S) connected to pressure gauges (RS PRO Dial, UK). Here, the FO testing method was adjusted to suit the capability of our FO laboratory setup. To determine the amount of permeated water, weight changes of the feed solution were accurately recorded using a digital balance (AND EK-3000i compact, A & D Weighing, U.S) at 5 min intervals. The water flux (J_w, **L/m^2.h, LMH**) was calculated as follows [40,41,44]:

$$J_w = \frac{\Delta V}{A.\Delta t} \quad (1)$$

Where (ΔV) is the volume change of the feed solution (in **L**) over a time interval (Δt in **h**), (A) is the effective area of the membrane (in **m^2**).

To assess the reverse solute flux (RSF) of the NaCl solution across the membrane to the feed solution side (DIW tank), the total dissolved solute (TDS) of NaCl in the feed solution was measured using a conductivity meter (FiveEasy™ Plus FP30, Mettler Toledo, Germany) over 2 h. The reverse solute flux (J_s, **g/m^2.h, gMH**) was calculated using [40,41,44]:

$$J_s = \frac{(C_t V_t) - (C_0 V_0)}{A.\Delta t} \quad (2)$$

Where (C_0 in **g/L**) and (V_0) are initial salt concentration and volume of feed solution, respectively, and (C_t in **g/L**) and (V_t) are the corresponding values of salt concentration and volume of feed solution over the operation time (Δt). Each experiment was repeated three times, and average results were reported in this study.

The specific salt flux (J_{sp} in **g/L**) of membranes, which is defined as the ratio of permeated NaCl solution to the amount of water permeation flow counter-currently across the membrane. This factor was determined by dividing the reverse solute flux over the water flux as follows [8,40,41]:

$$J_{sp} = \frac{J_s}{J_w} \quad (3)$$

To evaluate the salt rejection efficiency of membranes, the same FO configurational mode was used, however, 0.1 M of (1 L) NaCl and 0.5 M of (1 L) of dextrose aqueous dispersions were used as feed and draw solutions, respectively. Each salt rejection performance experiment was conducted for 3 h. The water flux (J_w, **L/m^2.h**) was similarly calculated by measuring weight changes using **equation (1)**. The percentage of salt rejection (R, %) was calculated using [40,41,44]:

$$R = \left(1 - \frac{C_p}{C_f}\right) \times 100 \quad (4)$$

Where (C_p) is the concentration of permeated salt from the feed solution to the draw solution, based on the corresponding mass changes of migrated water, (C_f) is the initial concentration of salt in the feed solution tank.

2.5. Structural stability testing of membranes

The dimensional stability and durability of as-fabricated membranes were tested under different mechanical and chemical conditions. The membranes were chemically tested for a certain duration by dipping samples into 0.6 M NaCl aqueous solution, representing the salt contents dissolved in a real seawater of 35.03 g. The NaCl solutions were stored in a dark place at 25 °C and replaced every 24 h to maintain a constant concentration. The exposure tests were conducted over different durations, and the chemical stability in the ionic solution was evaluated qualitatively as function of testing time.

To evaluate the long-term dimensional stability, beside monitoring the mechanical stability of membranes during FO desalination and hydraulic backwashing stages, the as-prepared membranes were also

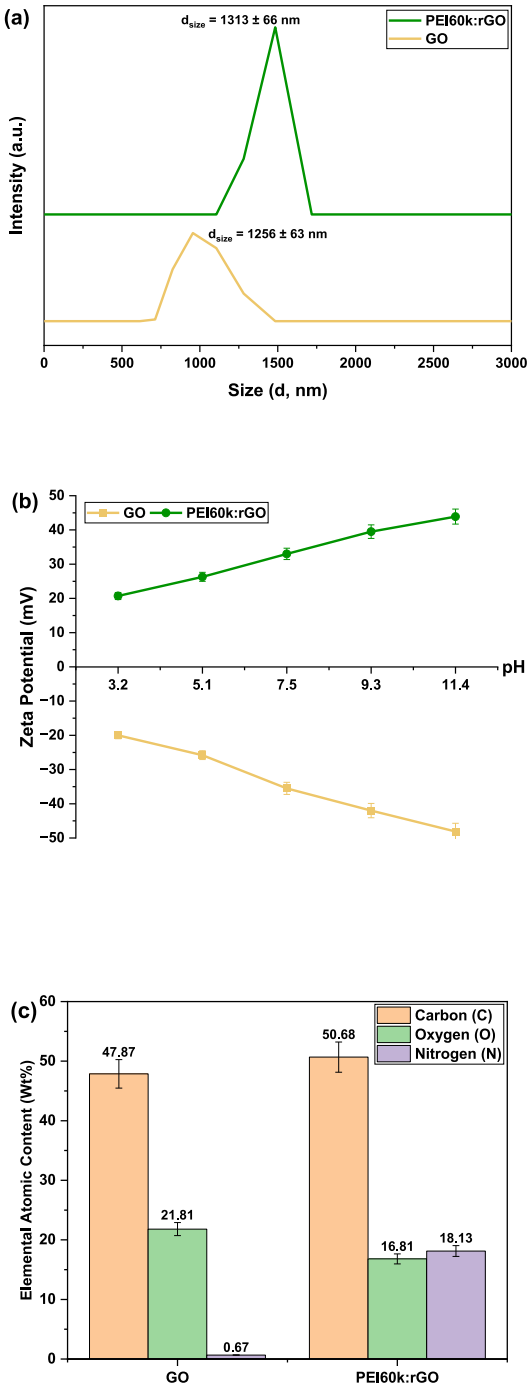

Fig. 2. **(a)** Hydrodynamic average size analysis, **(b)** surface zeta potential, and **(c)** chemical elemental compositions of GO and PEI60:rGO particles.

qualitatively tested by exposure to sonication in DIW using an ultrasonicator (*with ultrasonic frequency of* 80 Hz) over different periods. Again, the mechanical stability was also evaluated qualitatively as a function of exposure time. Moreover, the mechanical strength of membranes was also quantitatively evaluated through tensile testing and structural integrity assessments under rigorous testing conditions. Here, tension tests were carried out using a universal testing machine (Instron Model 3369), operating at a speed rate of 2.0 mm/min, applying a

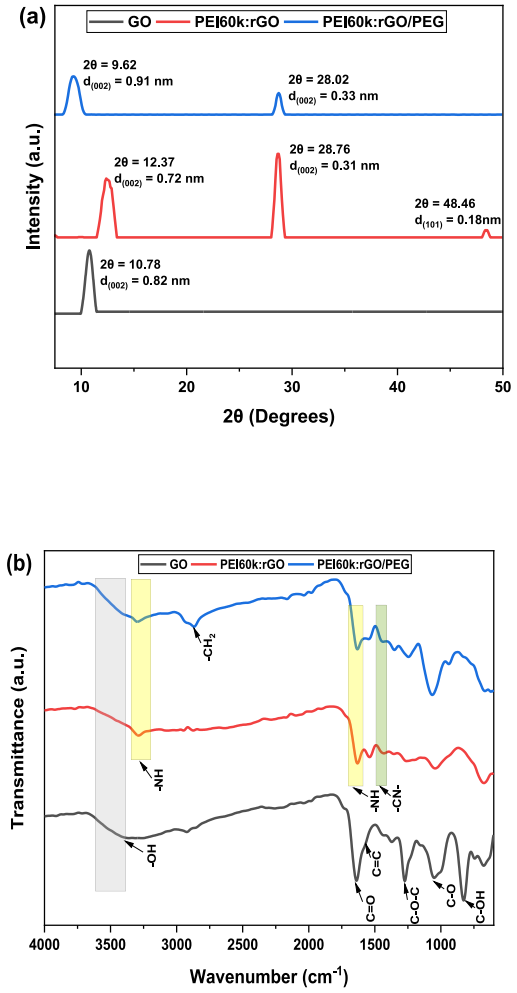

Fig. 3. **(a)** XRD spectra of interlayer spacing, and **(b)** FTIR spectra of functional groups of GO, PEI60k:rGO, and PEI60k:rGO/PEG membranes.

maximum load of 2.5 N. Before testing, the samples were carefully prepared by cutting them into strips measuring 0.5 cm × 5.0 cm.

3. Results and discussion

3.1. Characteristics of modified GO-based materials

The concentration of HPEI of 0.06 g/L was selected for preparation of a stable PEI60k:rGO dispersion to ensure uniformity with the membrane fabrication process, based on the optimisation procedure indicated in **Section (S1, SI)**. As can be described in Fig. 2 (a), DLS results for GO-based sheets demonstrated different size measurements than HPEI cross-linked rGO sheets. The average hydrodynamic diameter (HD) of GO laminates dispersed in water was approximately 1256 ± 63 nm. By 'grafting to' of the HPEI molecule, the size of the formed PEI60k:rGO sheet was enlarged to almost 1313 ± 66 nm. It is important to point out that the physiochemical properties and performance of the doped GO-based membranes can be significantly affected by the length of the HPEI molecule. This polymer has a longer molecular chain and more positive surface charge. These properties can easily keep the distance between GO layers tuned, and similarly retain stably electrostatic surface charges [18,34]. Accordingly, the HPEI can simultaneously have the potential to enhance salt rejection and retain an excellent water permeability of the as-prepared GO-based membranes.

Zeta potential (ZP) is a measure of the electrical surface charge of the membrane [45]. The ZP of GO and PEI60k:rGO laminates were measured at different corresponding pH, as shown in Fig. 2 (b). It was observed that the surface charge of GO laminates becomes more negative as the pH increases. This was because of the prompted deprotonation of carboxylic groups at the edges of GO sheet in water at higher pH [17,46]. This was also due to the acid modification of GO that resulted in more stable carbon groups with effectively obtained negative charges [16]. Similarly, PEI60k:rGO laminates demonstrated an increase in the surface charge with increasing pH due to increased protonation of carboxyl groups on GO sheets by HPEI molecules at higher pH [47,48]. As a result, the electro-positively charges retained by functionalising rGO laminates with HPEI can effectively provide an adequate electrostatic repulsion force to most common seawater ionic salts. In this work, PEI60k:rGO membranes were fabricated using a stable deposit at pH of 11.4.

To further investigate physicochemical characteristics of modified GO-based laminates, the CHNS–O analysis was conducted to confirm the successful functionalisation of the GO material using the HPEI. Fig. 2 (c) showed that the PEI60k:rGO composite confirmed the presence of carbon (C), nitrogen (N), and oxygen (O) elements with distinctive weight percentages compared to that of GO sheets, which relatively confirmed the presence of amine groups [47,49]. Whereas GO particles only showed C and O elements, where the percentage of oxygen was higher than that of the PEI60k:rGO sample, indicating the presence of sufficient oxidation for graphene [50]. The carbon-to-oxygen (C/O) ratio of the PEI60k:rGO was around 3, although GO laminates retained C/O ratio of 2.2. Therefore, the higher C/O ratio of PEI60k:rGO can be attributed to the reduction of oxygen-containing functional groups such as hydroxyl, carboxylic and epoxyl [28]. These findings were in line with EDX results shown in **Section (S3, SI)**. As a result, the interlayer spacing between rGO laminates would be subjected to decrease, and this can facilitate higher salt rejection performance for membranes. This was explained in more detail with the FTIR analysis of chemical structures for resultant membranes in **Section (6.2)**.

3.2. Characterisation of modified GO-based membranes

The interlayer spacing between GO-based laminates was examined using an XRD spectra analysis, as shown in Fig. 3 (a). It is noteworthy that d-spacing (i.e., nano-channel) plays an important role for fast transport of water molecules and sieving of ionic species [23,30]. The diameter of pathway between GO-based laminates can effectively determine the performance of the as-prepared membranes. The XRD profile of the prepared GO membrane exhibited a peak at 2 θ = 10.78° which was corresponding to a nano-channel distance of 0.82 nm [51], however, the PEI60k:rGO membrane showed three distinctive peaks at about 2 θ = 12.37°, 28.76°, and 48.46°, corresponding to nano-channels widths of 0.72, 0.31 and 0.18 nm. Accordingly, the reduction of d-spacing between modified rGO laminates was due to the removal of oxygen functional groups attached on the modified GO sheets after chemical functionalisation with the HPEI [43,52]. This led to the partial restoration of graphitic structure for the peak observed at 2 θ = 28.76°, which was supported by FTIR analysis. In addition, peaks shown at 2 θ = 12.37° and 48.46° were attributed to the presence of un-exfoliated GO and un-oxidised graphite material, respectively [43]. For the PEI60k:rGO/PEG membrane (*with an optimum PEG concertation of 0.*1 mg/mL, *as illustrated in* **Section (S2, SI)**), there was a peak observed at 2 θ = 28.02°, similar to that for the PEI60k:rGO membrane, which indicated a nano-channel width of 0.33 nm. Although, the intensity of that peak was reduced which could be attributed to the PEG infiltration through the structure of PEI60k:rGO laminates, and thus decreasing their crystallographic quality. Moreover, the peak observed at 2 θ = 12.37° for PEI60k:rGO laminates was shifted to lower value of 9.62°, revealing the increase in d-spacing of 0.91 nm after coating PEI60k:rGO laminates with PEG. This increase in the nano-channel width was due to high degree of PEG

molecular chain intercalation with the un-exfoliated GO and PEI60k doped rGO sheets, which is in agreement with the reported literature [53,54]. The effect of functionalisation approach, at which the PEG influenced the d-spacing between the cross-linked PEI60k:rGO laminates, was schematically illustrated in Fig. (S7).

Fig. 3 (b) shows the change in characteristic peaks of FTIR spectra for GO, PEI60k:rGO and PEI60k:rGO/PEG membranes. For the structure of GO laminates, there were characteristic signal peaks observed at approximately 760 cm^{-1}, 1080 cm^{-1}, 1260 cm^{-1}, 1580 cm^{-1}, 1690 cm^{-1} and 3475 cm^{-1} which corresponded to skeleton vibrations of C–OH, C–O, C–O–C stretching, C–C small stretching, C═O stretching and –OH stretching, respectively [42,55,56]. It was obvious that the hydroxyl groups were partially reduced after treatment with the HCl acid to create a stable carbon framework for further functionalisation with other nanomaterials [16]. Accordingly, it was expected that C═O, C–O–C or C═C skeleton vibrations were mostly dominating the reaction between the GO and hydrogen bonding of the acid molecule [42,57]. This can be confirmed by increasing signals intensity of C═O and C–O–C stretching. It is important to reveal that HCl, under thermal conditions of 40 °C, can facilitate slightly the partial reduction of GO oxygen-containing functional groups, particularly epoxyl and hydroxyls [42]. The acidic condition created by HCl can also help removing metal ion impurities which might be present in the GO from the oxidation process of the graphite during the synthesis of GO [58]. These metal ions could interfere with subsequent chemical reactions, and it is accordingly vital to remove them. When the GO surface is ensured to be clean from impurities, the HCl treatment can ensure that functional groups are more uniformly distributed and accessible, leading to a stable carbon structure, which is crucial for effective functionalisation with HPEI molecules. Furthermore, HCl, under a treatment temperature of 40 °C, could also facilitate dehydration reactions, where water is removed from adjacent hydroxyl groups, leading to the formation of additional C═C bonds [42,58–60]. This process can further contribute to the restoration of the sp^2 carbon network, enhancing the stability of the GO. These dehydration and condensation reactions could be useful for preparing more suitable GO structure for subsequent chemical modifications. The more graphitic structure of GO formed after the acid treatment would be more compatible with the functionalisation with HPEI molecules, resulting in better bonding and more stable GO laminates. This reaction can effectively link the HPEI covalently to the GO structure, creating a stable amide bond between the two molecules. After crosslinking and modification with amino groups of HPEI molecules, the structure of PEI60k:rGO laminates had possessed new peaks at around 1357 cm^{-1}, 1570 cm^{-1}, and 3250 cm^{-1} which were related to –CN bond in the secondary amine, –NH bond in the abundant secondary amine and –NH bond in the primary amine groups, respectively [61,62]. In addition, FTIR spectra of the HPEI doped rGO membrane exhibited a reduced structure of carbonyl/carboxylic groups and almost removal of epoxy contents [34]. This can illustrate that amine groups of the HPEI had reacted with epoxy and carbonyl/carboxylic groups of the treated GO through a covalent bonding during crosslinking reactions, as follows: GO-COOH + HPEI-NH_2 → GO–CONH–HPEI + H_2O [34,49,62]. Therefore, the expected structure in Scheme (S1, SI) elucidated that there could be only two amine groups from the HPEI molecule to react with the GO, as indicated by the presence of amine groups in the FTIR spectrum for the PEI60k:rGO composite. As a result, the surface of the GO had been imparted with further partial reduction of oxygen-functional groups and obtained abundant positive charge by amine groups of HPEI, which can further enhance material's properties and effectively facilitate a high desalination performance. After coating of PEI60k:rGO layers with PEG molecules, it was clearly observed that there were no changes in the intensity of pre-existing primary and secondary absorption bands of amine groups. In addition, one newly intense peak at around 2830 cm^{-1} was detected, which was corresponding to $–CH_2$ [36,54]. Also, the intensity of C–O stretching band at 1090 cm^{-1} was significantly elevated for the PEI60k:rGO/PEG membrane compared to that of the PEI60k:rGO. Therefore, this can be evident the PEG was successfully grafted onto both HPEI molecules and modified rGO laminates between two adjacent amide bonding by the esterification reaction with -OH bond on the surface of PEI60k:rGO sheets. From this point, it was suggested that the chemical structure of the PEI60k:rGO/PEG membrane could involve reaction of one amid group of PEG molecules, which could be perpendicularly cross-linked with two parallel HPEI doped rGO sheets through non-covalent interactions (*both electrostatic interaction and weak van der Waals force*).

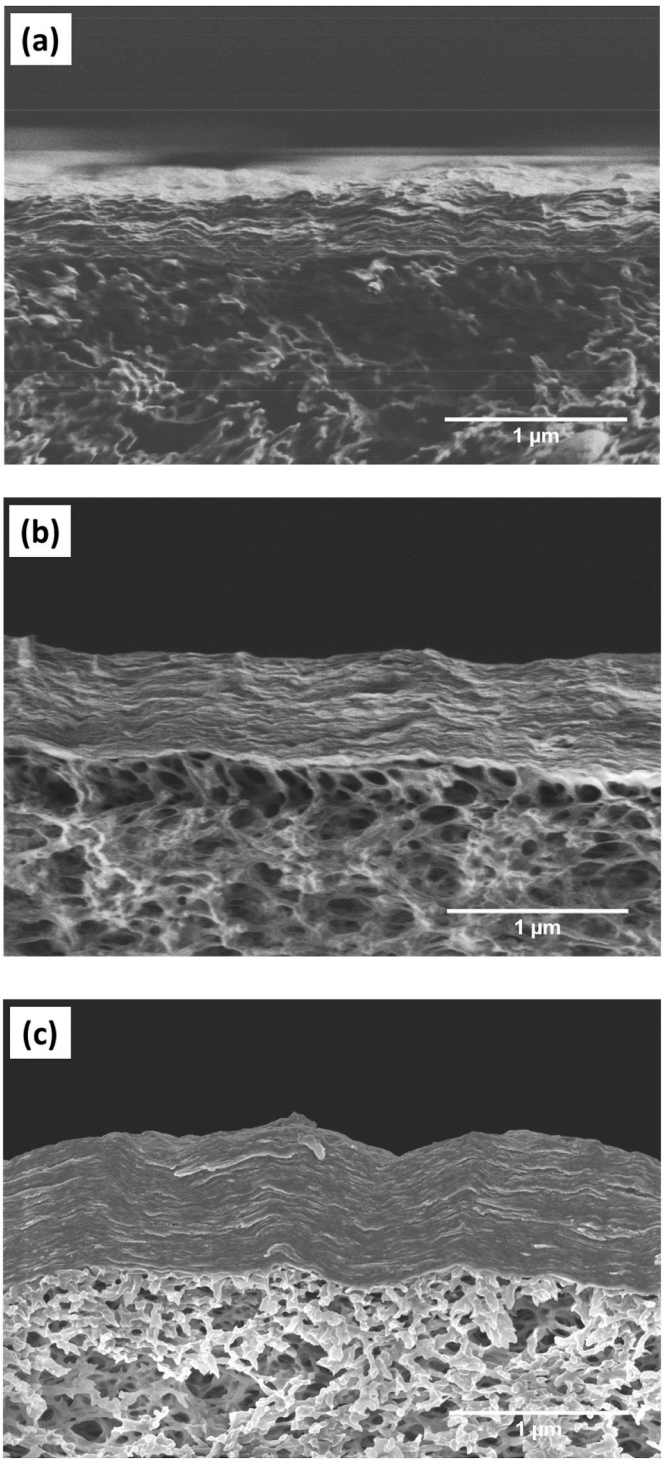

Fig. 4. SEM cross-section of microstructures of **(a)** GO, **(b)** PEI60k:rGO, and **(c)** PEI60k:rGO/PEG membranes.

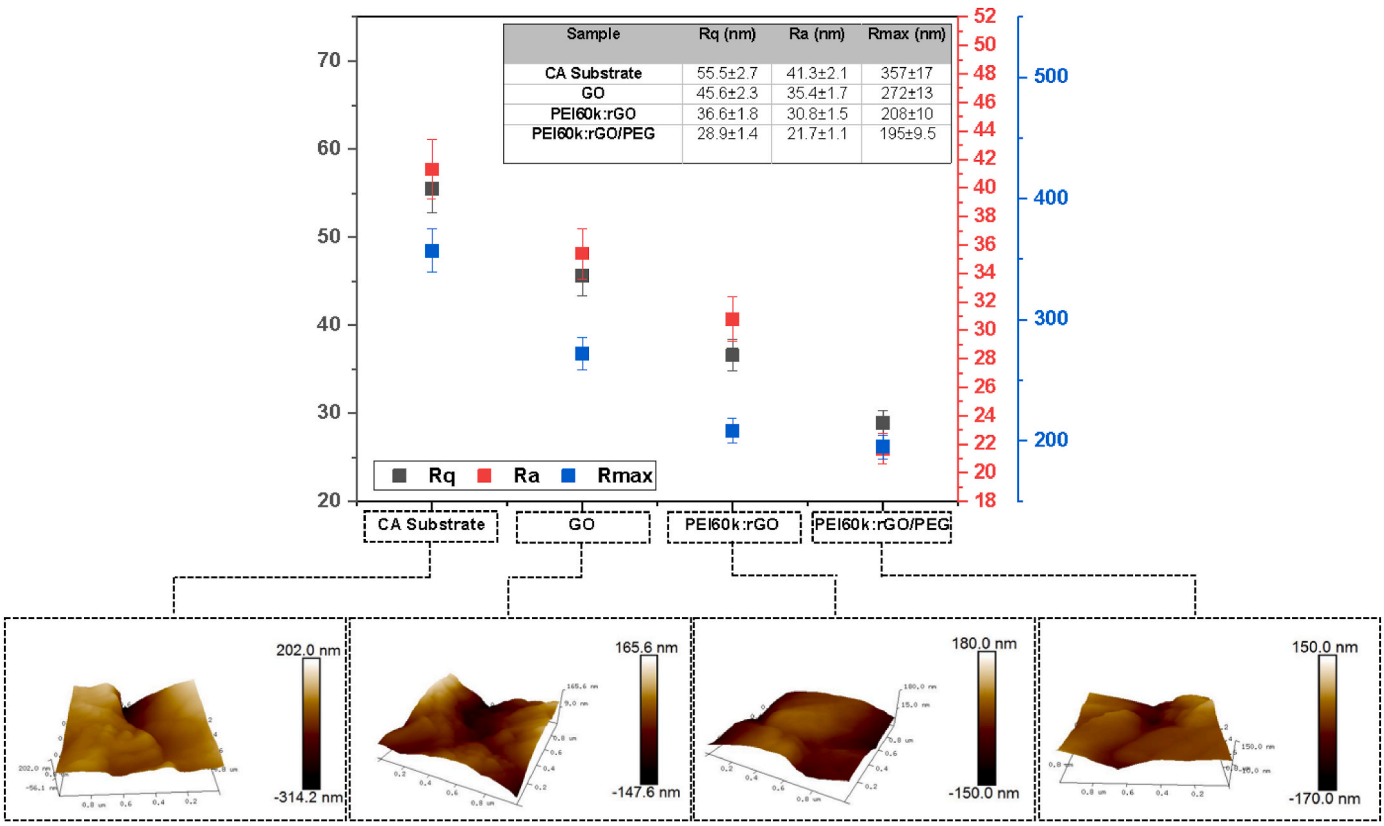

Fig. 5. AFM measurements of CA substrate, GO and rGO modified membranes.

This can enhance the surface wettability and stability of the PEI60k: rGO/PEG membrane.

Assessment of surface morphology allows determination of the surface structure of deposited materials on the membrane. As can be seen in Fig. S8 (a) and **(b)**, the commercial CA substrate exhibited a highly porous and rough surface [63]. After deposition of GO-based layers on the CA membrane, it was clear that uniform GO-based films were successfully fabricated without visible defects, forming typically wrinkled-like structures for GO laminates [16], as seen in Fig. S8 (c - h). It should be noted that the surface of GO-based membranes exhibited less rough morphology after cross-linking and modification with HPEI and PEG molecules, simultaneously, confirming the change in their chemical structures as illustrated in FTIR spectra. Also, it was observed that the surface morphology of GO-based membranes had no visible pores, even for magnified SEM images, which could be formed in a nanoscale size. Besides, this could prove that the interlayer spacing can be the dominant pathway to facilitate molecular/ionic transport across GO-based membranes [34].

In terms of thickness of deposited layers, the GO membrane demonstrated the thinnest layer (402 ± 20.1 nm), followed by PEI60k: rGO (570 ± 28.5 nm) and PEI60k:rGO/PEG (740 ± 37 nm) membranes, as shown in Fig. (4). It should be noted that, in our work, the thickness of all functionalised GO-based membranes increased gradually after modification with HPEI molecules. This could be attributed to an increase of the thickness of PEI60k:rGO laminates, compared to that of the GO after crosslinking, but with a reduced interlayer spacing as shown in XRD patterns. Besides, a further increase with the thickness of the PEI60k:rGO/PEG film was also observed, which was due to the intercalation of PEG molecules between PEI60k doped rGO laminates, resulting in slight increase in their d-spacing, as agreed with XRD results in Fig. 3 (a).

Surface topography measurements, in terms of surface roughness, were performed using AFM to further characterise the surface

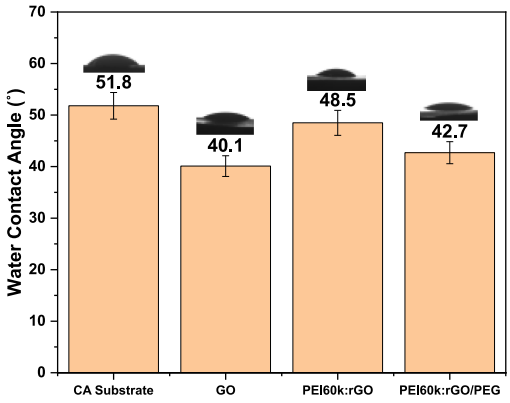

Fig. 6. Water contact angle measurements of CA substrate and GO-based membranes.

morphology of membranes. As shown in Fig. (5), the PEI60k:rGO/PEG membrane demonstrated the lowest surface measurement, followed by PEI60k:rGO, GO and CA support membranes. After the deposition of GO laminates onto the CA support layer, the average surface roughness was slightly reduced due to the presence of hydrophilic oxygen-containing functional groups within the chemical structure of the GO. When GO laminates were modified by the amine-based HPEI, the average roughness was decreased and thus defects on the GO surface were covered due to the change in the chemical structure of membranes [64,65]. In addition, a further decrease in the surface roughness was observed after coating with the PEG, due to the intercalation of more amine groups

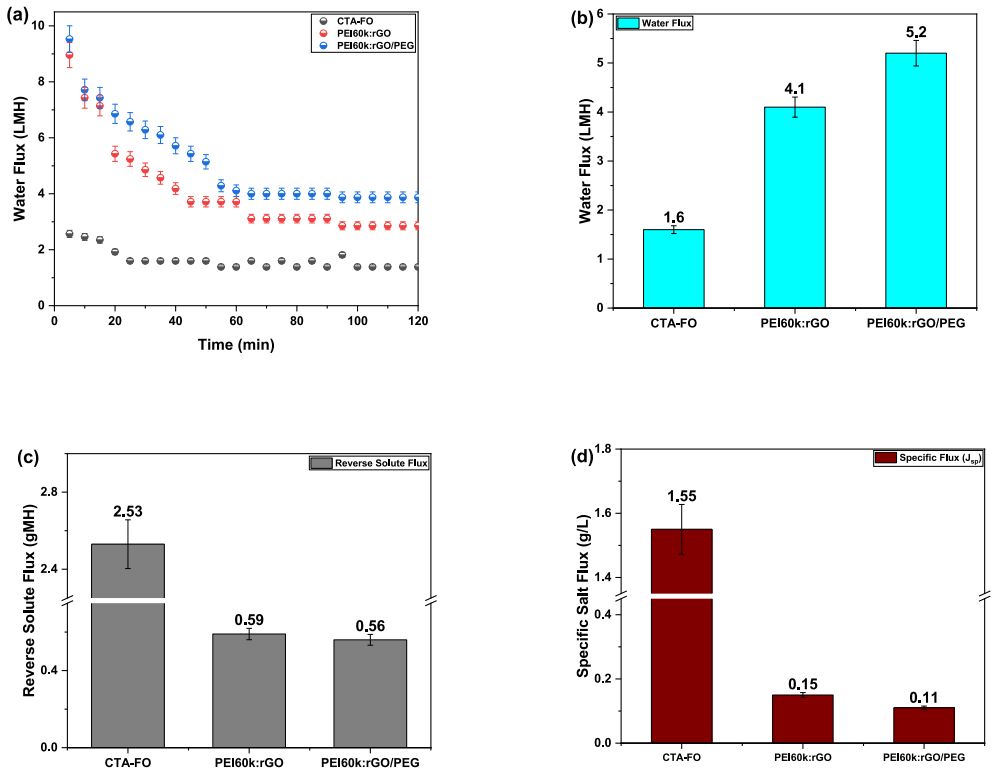

Fig. 7. Lab-scale FO performance test: **(a)** Water permeation trends, **(b)** Average water flux, **(c)** Reverse solute flux, and **(d)** Specific salt flux of commercial CTA-FO, PEI60k:rGO and PEI60k:rGO/PEG membranes. [DI water and 0.6 M NaCl ionic solution were selected as feed and draw solutions, respectively].

[54]. The findings agreed with observations from SEM images (see Fig. S8, SI).

The surface hydrophilicity also plays a key role in the desalination performance and anti-fouling property of the membrane. Water contact angle measurements of CA support and GO-based membranes were presented in Fig. (6). It was observed that hydrophilicity of the CA substrate was increased after the coating with the GO, due to presence of abundant oxygen functional groups. However, the wettability of the PEI60k:rGO membrane was decreased after functionalisation of GO with the HPEI, due to the reaction of GO oxygenated-carboxyl groups with HPEI amine groups [34]. Therefore, the WCA measurement of the HPEI crosslinked rGO membrane was increased. In comparison, the wettability of PEI60k:rGO doped PEG membrane was further increased, owing to the addition of more amide groups on the surface of PEI60k:rGO/PEG membrane, which confirmed obtained results from FTIR analysis. It should be noted that, despite the reduction of wettability of cross-linked rGO membranes compared to that of the GO, the amount of hydrophilic oxygen-functional groups on their surfaces can be still sufficient in the range of hydrophilic surfaces to provide a good water permeability [32, 64].

3.3. Evaluation of rGO membranes performance in an FO desalination

Performance of the as-prepared rGO-based membranes, compared to the commercial CTA-FO membrane, was initially assessed by measuring water flux and reverse solute flux in FO-based membrane system under same conditions, as presented in Fig. (7). Fig. 7 (a) showed that the water flux trend of the PEI60k:rGO/PEG membrane was higher than that of the PEI60k:rGO and CTA-FO membranes, at which it exhibited a more stable water permeation after around 55 min than the other tested membranes in the FO process. In addition, the PEI60k:rGO film was seen to achieve the highest average water flux, followed by PEI60k:rGO and commercial CTA-FO membranes, as quantitatively presented in Fig. 7 (b), which is in agreement with the reported literature [66]. This confirmed that the intercalation of PEG molecules, through the surface, into the microstructure of the PEI60k:rGO membrane effectively improved its hydrophilicity and provided low-friction hydrophobic nano-channels, which supported WCA measurements and SEM observations. Although, it should be pointed out that the micrometre thickness of resultant rGO membranes was obviously the barrier for their low water permeation, nevertheless, it could be beneficial for reduction of ions selectivity.

As rGO-based membranes involved the use of a support layer (i.e., CA substrate), the ICP effect was evaluated by measuring the reverse solute permeation across membranes, as shown in Fig. 7 (c). The average reverse solute flux of the PEI60k:rGO membrane was less than that of PEI60k:rGO and CTA-FO membranes, as a results of HPEI and PEG modification reactions with the GO. For both modified rGO-based membranes, the interaction between HPEI and GO sheets facilitated the fast forward water transport. Also, it prevented the occurrence of a high concentration difference between feed and draw solution sides near the membrane surface, and hence lowering the effective osmatic pressure across membranes [20], owing to its tuned inter-layer spacing and possessed Donnan exclusion effect [18,67]. This was observed to be further enhanced by the deposition of hydrophilic PEG, which confirmed results for obtaining higher water flux for the PEI60k:rGO/-PEG membrane compared to other tested membranes. Resultant observations were confirmed by calculating the specific salt flux, as seen in Fig. 7 (d). It can be described that the specific salt flux of the PEI60k:rGO/PEG membrane induced the lowest value, compared to that of the PEI60k:rGO and commercial CTA-FO membranes. This implied that the PEI60k:rGO/PEG membrane achieved least effects of the ICP phenomenon.

To further evaluate the ion permeability across tested membranes, the same FO system was used under same conditions (*with DI water and 0.6 M NaCl solution selected as feed and draw solutions, respectively*). Fig. (S9) indicated trends of the NaCl concentration permeated across all membranes as a function of testing time. Amongst membranes, the CA

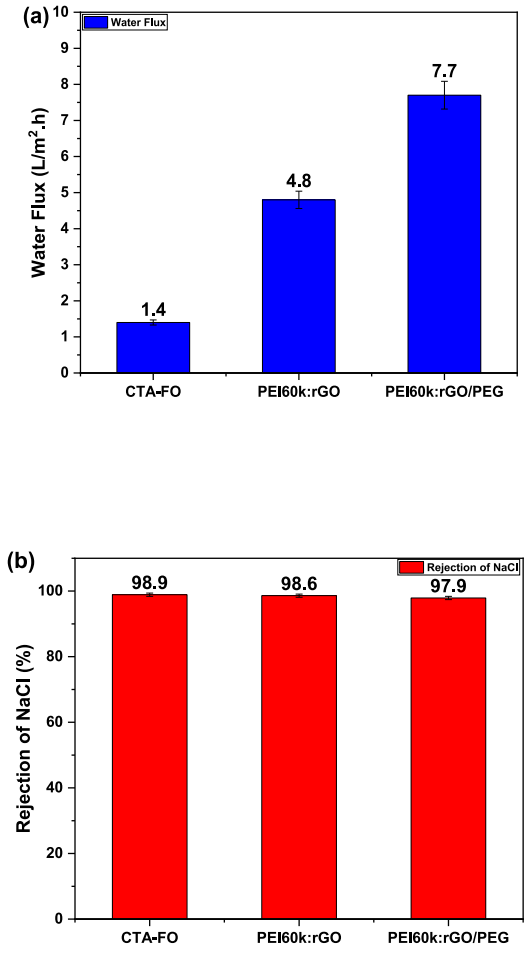

Fig. 8. Lab-scale FO desalination performance test: **(a)** Water permeation and **(b)** Percentages of salt rejection of GO and rGO modified membranes compared to the CTA-FO membrane. [0.1 M NaCl solution and 0.5 M dextrose were used as feed and draw solutions, respectively].

substrate was the most permeable to Na^+ and Cl^- ions from draw to feed sides, as seen in Fig. S9 (a). After deposition of the GO layer onto the CA support layer, the ion permeability of the GO membrane was decreased by almost 95 %. It was also observed in Fig. S9 (b) that resultant rGO-based membranes (i.e., both HPEI- and HPEI/PEG-rGO) exhibited lower ion permeation rates (around 78 % and 26 %, respectively) than that of GO and commercial CTA-FO membranes, respectively. This was attributed to their tightened interlaminar spacing, micrometre thickness and active Donnan effects near the surface of membranes. On the other hand, it was found that there was a very slight change in the permeation of ions between as-fabricated rGO-based membranes, which accordingly agreed with results of the reverse solute flux. Therefore, obtained ion permeation results proposed that rGO-based membranes can effectively provide higher salt rejections than GO and commercial CTA-FO membranes for FO desalination.

To evaluate the salt efficiency of membranes in FO desalination system, 0.1 M NaCl and 0.5 M dextrose were employed as feed and draw solutions, respectively. As seen in Fig. 8 (a), the PEI60k:rGO/PEG membrane demonstrated the highest water permeation followed by PEI60k:rGO and CTA-FO membranes, which agreed with obtained results of the ICP- FO evaluation under same FO conditions. However, the salt rejection performance of the PEI60k:rGO/PEG membrane showed slightly higher ion diffusivity rate than that of the PEI60k:rGO membrane, confirming more forward salt ions permeated across the membrane from the feed side to the draw side. In comparison, the CTA-FO membrane exhibited the highest salt rejection efficiency, which is in line with the reported literature [16,20].

To further understanding the conceptual mechanism of salt rejections for the resultant rGO-based membrane, the effect of membrane charge was further investigated. It is noteworthy that the charge on the surface of membrane can have a significant role on the electrostatic repulsion of charged ions (*i.e., Donnan exclusion theory*), as reported in the literature [18,28,34,67]. In this study, the electroneutrality of resultant HPEI doped rGO laminates on surfaces of membranes was well maintained to reject charged co-ions. Herein, the PEI60k:rGO surface possessed a positive charge of +43.6 mV (*with* pH *11.4*), but the PEG solution had a much weaker positively surface charge of +9.3 mV, according to the obtained ZP results. Therefore, the PEI60k:rGO membrane was suggested to have stronger electrostatic repulsion force which could reject more cationic species (i.e., co-ions of Na^+) than that of the PEG coated PEI60k:rGO membrane. As such, the infiltration of PEG was firstly proposed to be the reason for slightly diminishing the salt rejection efficiency of the PEI60k:rGO/PEG membrane. The second potential reason could be that the intercalation of the PEG material induced d-spacings to be increased between PEI60k:rGO laminates, as observed in XRD results, compared to those without PEG coating. This could lead to the permeation of more hydrated ions across the PEG coated PEI60k:rGO membrane from feed solution to draw solution sides. Fig. (9) represents expected conceptual mechanisms for improving desalination performance, in terms of water flux and salt retention, across the as-prepared PEI60k:rGO/PEG membrane.

To further assess the desalination performance of tested rGO membranes in an FO process, the FESEM-EDX analysis of sieving forward ions (i.e., Na^+ and Cl^-) was required, as depicted in Fig. (S10). It was observed that the atomic weight percentage of Cl^- ions on the surface of the tested PEI60k:rGO membrane was higher than that of the PEG coated PEI60k:rGO membrane. This could be attributed to strong electrostatic attractions between the positively charged surface of the PEI60k:rGO membrane and negatively charged Cl^- ions, resulting in a cake-formation of excess Cl^- co-ions on the surface of the membrane [68], as seen in Fig. S10 (a). Therefore, this could significantly contribute to reduce the forward water flux across nano-channels of the PEI60k:rGO film, which could confirm obtained results from the FO desalination. On the other hand, as presented in Fig. S10 (b), the PEI60k:rGO/PEG membrane showed a lower amount of Cl^- elements but slightly higher quantity of Na^+ elements than that of the PEI60k:rGO membrane. This may confirm our proposed hypothesis of intercalating PEG molecules into PEI60k:rGO sheets, and their effects for enhancing water permeation and lowering the salt rejection. Despite these findings, the PEI60k:rGO/PEG membrane can still be promising in the FO application because of its excellent desalination performance.

3.4. *Structural integrity assessment of modified GO membranes*

Since mechanical and chemical washing processes are regularly required to recover the performance of FO membranes, the stability of GO-based laminates has been a bottleneck for their practical applications. To assess the long-term dimensional durability and integrity of as-fabricated membranes, GO and rGO-based membranes were firstly assessed by immersing in 0.6 M of the NaCl ionic solution, as shown in Fig. (10) (*Supported by* Fig. (S11)). It can be observed that the GO membrane was detached from the CA substrate and started to disintegrate from day 1, until completely destroyed within less than one week. Contrastingly, the structure of the PEI60k:rGO membrane demonstrated a well-maintained stability for almost 4 weeks. In comparison, after coating of PEI60k:rGO sheets with the PEG, the stability and structural durability of the resultant membrane were further improved and maintained for more than 6 weeks without any visible damages. The

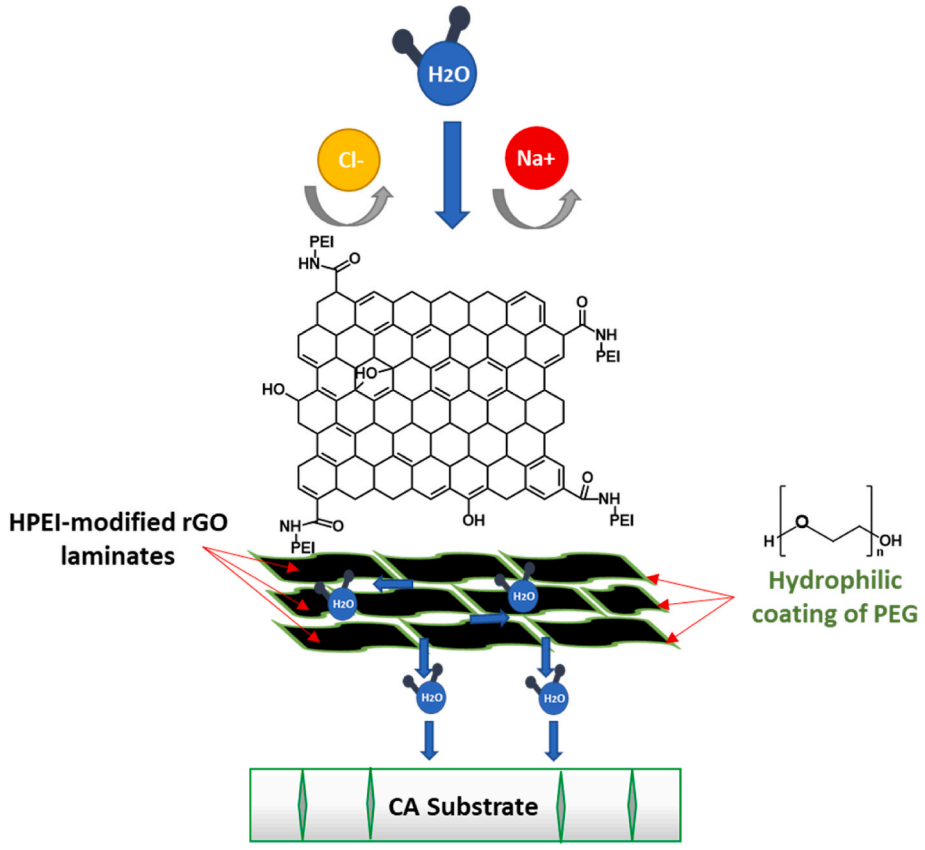

Fig. 9. Schematic diagram of possible mechanisms for improving desalination performance (i.e., water flux and salt rejection) across the PEI60k:rGO/PEG membrane (*along with possible chemical structures*) [43,49,62], where water molecules are attracted by PEG coated PEI60k:rGO laminates and transported through ultra-fast hydrophobic nanochannels by the capillary force, while charged feed ions are being rejected by size exclusion and electrostatic repulsion forces near the surface of the membrane.

	(Exposure Time in 0.6 M NaCl)			
Membrane	**1 day**	**1 week**	**< 4 weeks**	**≥ 6 weeks**
GO	2	0	-	-
PEI60k:rGO	5	4	3	-
PEI60k:rGO/PEG	5	5	5	4

Excellent (Score: 5) Good (Score: 4) Fair (Score: 3-2) Poor (Score: 1-0)

Fig. 10. Stability evaluation of GO-based membranes based on an industrial rating scheme, dipped in 0.6 M of NaCl solution as a function of time.

	(Structural durability in ultrasonication)		
Membrane	**< 5 min**	**< 20 min**	**< 50 min**
GO	0	-	-
PEI60k:rGO	3	1	-
PEI60k:rGO/PEG	5	5	4

Stable (Score: 5) Disassembled (Score: 4)
Deformed (Score: 3-2) Critically damaged (Score: 1-0)

Fig. 11. Structural durability evaluation of GO-based membranes, exposed to ultra-sonication based on an industrial rating scheme.

obtained observations can confirm that the excellent stability of PEI60k:rGO/PEG was due to the tight bonding between PEG and HPEI doped rGO sheets. In the case of the PEI60k:rGO membrane, some of HPEI molecules formed tail bonding between two neighbouring GO sheets, resulting in an insufficient force to tightly maintain the structure of the membrane. As a result of the limiting effect of sodium ions, the PEI60k:

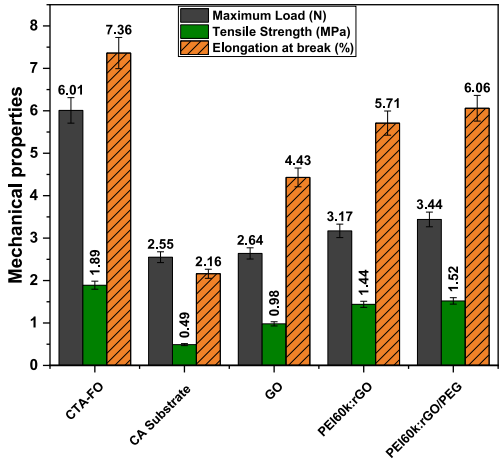

Fig. 12. Assessment of the mechanical integrity and durability of membranes *via* tensile strength testing.

rGO membrane started to loss its initial structure and stability after a certain time of exposing in the ionic solution [29,44].

To evaluate the structural integrity and durability of membranes, GO and rGO films were also compared by testing them in a harsh condition under ultrasonication for a certain duration. As can be observed in Fig. (11) (*Supported by* Fig. (S12)), the GO membrane was not separated from the CA substrate but easily deformed in a short testing time. On the other hand, the PEI60k modified rGO membrane maintained a good stability in the sonicator for about 20 min, owing to strong interactions between the GO and crosslinked HPEI molecules [18,34]. In comparison, the PEI60k:rGO/PEG membrane demonstrated the best durability and stability and remained unchanged for more than 50 min. As proposed, PEG molecules played a vital role to further stabilise stacked PEI60k:rGO laminates, as well-agreed with the reported literature [35].

The structural integrity of GO-based membranes was also investigated during the FO performance process. As expected, the GO membrane easily lost its integrity and, hence, its FO performance was not considered in this study, for any comparison with other modified rGO membranes. On the other hand, the modified rGO membranes showed an excellent stability for 3 h during FO performance evaluation tests. Therefore, it can be concluded that the successful functionalisation between HPEI, and modified GO laminates significantly improved the structural integrity of modified rGO membranes. This was further enhanced with addition of PEG molecules. As such, the PEG was well-maintained the stability of the PEI60:rGO membrane by providing a strong attraction between HPEI modified rGO laminates.

Membranes predominately encounter shear stresses due to the friction between its surface and cross-flowing fluids, particularly in an ideal FO system [69–71]. Several factors can influence the performance of FO membranes, including properties of raw materials, fabrication techniques and parameters, the inclusion of doping additives, and structural characteristics such as porosity and tortuosity [72]. Therefore, it is crucial to further investigate the dimensional stability of membranes in more vigorous conditions. To assess mechanical properties of fabricated membranes relative to commercial CA substrate and CTA-FO membranes, various tests for quantifying the mechanical integrity, including maximum load, tensile strength, and elongation at the break, were performed, with that results presented in Fig. (12) and Fig. (S 13). It is important to highlight that commercial CTA-FO membranes typically demonstrate superior chemical and mechanical stability across various pH levels and under mechanical stresses, with a minimal degradation [73–76]. It was observed that the CTA-FO membrane demonstrated the highest maximum load, tensile strength, and elongation at break compared to other tested membranes, reflecting its ability to resist breaking coupled with significant flexibility under tension and before rupture. This is due to its dense structure and well-integrated cellulose triacetate polymer matrix of typically manufactured phase inversion-based CTA membranes [41,76]. This observation aligns well with our stability performance assessments of the commercial CTA-FO, as detailed in Fig. (12) and as reported in our previous work [41]. In comparison, CA membranes, which were used in this work as support layers to GO and rGO modified membranes, exhibited the lowest mechanical strength under tension conditions (Fig. 12). Typically, CA membranes show lower mechanical stability and flexibility due to their inherent material properties and presence of more voids within their structure which weaken the material, and this can limit their application under high-stress conditions [77]. After the incorporation of GO onto the top of CA substrates using a vacuum filtration, this likely reduced the effective porosity of the membrane by filling pores and providing a more uniform surface, beside the inherent mechanical stability of GO material. This could explain that there was observed a slight increase in mechanical strength and flexibility (Fig. 12), as GO laminates may bridge and reinforce the porous structure of the CA support, resulting in a more cohesive material on the membrane. A Further increase in the mechanical strength and stability was demonstrated when HPEI and rGO were synergistically doped, as the HPEI provided strong intermolecular interactions when crosslinked with the GO, which contributed to the enhancement of the structural integrity. Therefore, the PEI60k:rGO membrane showed an improved tensile strength and mechanical properties compared to the GO-coated membrane (Fig. 12). This suggests that the introduction of HPEI with rGO likely to further reduce the porosity by filling more of voids and creating more compact and uniform structure, and interconnected network within the membrane [18,34]. The mechanical strength and flexibility of PEI60k:rGO membrane was further improved after the infiltration of the PEG, which could explain the slightly more increase in the tensile strength, as depicted in Fig. (12). Infiltrating the PEG into the structure of the PEI60k:rGO membrane provided a strong attraction between HPEI modified rGO laminates, which could be explained by decreasing the porosity of the membrane, created a slightly denser structure but provided a more hydrophilic nature [35]. The obtained results of mechanical properties are well-aligned with qualitative findings of chemical and mechanical stability assessments of GO-based and rGO modified membranes.

To further elaborate on the mechanical stability of rGO coated CA membranes, the thermo-dynamic compatibility between functionalised polymers (i.e., HPEI and PEG) and CA polymer substrates could be evaluated by considering the Flory-Huggins interaction parameter, which is a measure of the interaction between different polymer species [78,79]. When the interaction parameter is considered to be low, it indicates better miscibility and hence, better compatibility between doping polymers and the substrate [80–82]. This improved compatibility can enhance the mechanical stability of membranes [78]. For binary interactions, the Flory-Huggins parameter typically should be less than 0.5 [79,80]. It should be important to state that the reduction in oxygen-containing functional groups of GO and the presence of amine groups from the HPEI could form hydrogen bonds and interact electrostatically with hydroxyl groups of the CA substrate [83]. These interactions are favourable, which is likely proposed to lead to a lower interaction parameter than 0.5, implying good compatibility. This could reveal that the PEI60k:rGO coating will adhere more strongly to the CA substrate. This was proposed to reduce the likelihood of mechanical failure during FO cross-flow operations. This strong interaction between polymer layers could also help to maintain the integrity of the membrane under harsh conditions (i.e., stress), enhancing its mechanical stability. Infiltering the PEG into the PEI60k:rGO structure introduced additional hydrophilic groups, which could be potentially altering the interaction with the CA substrate [83,84]. PEG chains can interact with both the CA substrate and the PEI60k layer through hydrogen bonding and van der Waals forces, as stated in **Section 3.2**. The presence of PEG was proposed to further decrease the interaction parameter (>0.5) due

Table 1
Comparison of water permeation and NaCl salt rejection of rGO-based membranes, being evaluated in a lab-scale FO desalination system.

Membrane/Substrate	Feed concentration (M)	Thickness of deposited rGO layer (nm)	Water flux (LMH)	NaCl rejection (%)	Reverse solute flux (gMH)	Ref.
PEI60k:rGO/CA	0.1	~570	~4.8	98.6	0.59	**This work**
PEI60k:rGO-PEG/CA	0.1	~740	~7.7	97.9	0.56	**This work**
rGO/MCE	0.1	~159.7	~37.5	96	4.67	[28]
pDA-rGO/MCE	0.1	~170.4	~46.9	92	2.62	[28]
rGO-AgNPs-pDA/MCE	0.03	~150	~18.3	65.6	4.96	[20]
rGO/MCE	0.03	~150	~13.9	63	4.21	[20]
rGO/CNT	0.009	~51	~2.11	96.6	1.52	[17]
rGO/PES	0.009	~51	~2.02	95.7	1.48	[17]

to its differently chemical nature compared to CA and HPEI, which could be well-integrated into the PEI60k:rGO matrix, and hence formed a stable coating with the CA substrate. This could ensure high compatibility and mechanical stability, which aligned well with quantitative and qualitative assessments for the chemical and mechanical stability of modified rGO membranes.

To establish a better understanding of the obtained results, water flux and salt rejection parameters of the as-prepared rGO membranes (in this work) were compared to other recently developed rGO-FO membranes which have been reported in the literature. These comparisons were thoroughly summarised in **Table (1)**. As can be clearly described, the salt rejection efficiency of our prepared rGO membranes outperformed that of the other membranes, however, our water permeation rates were slightly compromised compared to the reported literature. In addition, the comprehensive evaluation of the long-term chemical and mechanical stability of rGO-based FO membranes in the current literature remain limited [40,41,85].

4. Conclusion

The facile fabrication of the PEI60k:rGO/PEG membrane was successfully performed *via* a novel two-step chemical procedure. This firstly included the construction of stable carbon-based GO frameworks by the acid treatment with HCl, followed by reduction and crosslinking of acid-treated GO with HPEI molecules. The last step involved the hydrophilic modification with a low concentration PEG solution. As a result of functionalisation and modification reactions, simultaneously, the as-prepared rGO membranes possessed highly stable microstructures, tightened inter-layer spacing between modified GO laminates, and sufficiently hydrophilic surfaces. The synergistic effect of HPEI and PEG within the PEI60k:rGO/PEG membrane structure significantly improved its water absorption rate and salt retention efficiency towards charged salt ions. In FO desalination tests, the as-fabricated PEI60k:rGO/PEG membrane clearly demonstrated around 37 % and 82 % higher water flux rates than PEI60k:rGO and CTA-FO membranes, respectively, with significantly improved rejection performance for forward and reverse solute fluxes. Furthermore, the resultant membrane exhibited excellent mechanical and chemical stability through evaluating its structural durability in harsh conditions and ionic solutions. This study can be the breakthrough for development of new rGO-based membranes for the practical application of FO desalination. Therefore, future studies should focus on optimising concentration of the PEG for more permeability and stability enhancements. Moreover, the thickness of modified rGO layers needs to be controlled to further improve water permeability rates while maintaining an excellent selectivity of small molecular ions. Besides, Future research should also focus on further investigation and optimisation, such as enhancing the surface modification to improve anti-fouling capabilities.

CRediT authorship contribution statement

Mohamed Edokali: Writing – review & editing, Writing – original draft, Validation, Methodology, Investigation, Formal analysis, Data curation, Conceptualization. **Rachel Bocking:** Writing – review & editing, Investigation, Formal analysis. **Alexander Massey:** Writing – review & editing, Investigation. **Abdulhakim Al Hinai:** Writing – review & editing, Investigation. **David Harbottle:** Writing – review & editing, Supervision. **Robert Menzel:** Writing – review & editing, Supervision, Methodology, Investigation, Formal analysis, Conceptualization. **Ali Hassanpour:** Writing – review & editing, Supervision, Methodology, Investigation, Formal analysis.

Declaration of competing interest

The authors declare that they have no known competing financial interests or personal relationships that could have appeared to influence the work reported in this paper.

Data availability

Data will be made available on request.

Acknowledgment

The authors would like to acknowledge the financial support from the Ministry of Higher Education and Scientific Research – State of Libya. We also acknowledge the technical support provided by Dr Ben Douglas, Dr Christopher Hodges, Dr Adrian Cunliffe, Dr Karine Alves, Mr Mohammed Javed, and Mr David Instrell from the school of chemical and process engineering (University of Leeds), Mr Stuart Micklethwaite from Leeds Electron microscopy and spectroscopy centre (LEMAS), and Dr Christopher Pask from the school of chemistry (University of Leeds).

Appendix A. Supplementary data

Supplementary data to this article can be found online at https://doi.org/10.1016/j.polymer.2024.127644.

References

[1] U.N.D. Programme, Kenya National Human Development Report, vol. 5, United Nations Development Programme, 2006.
[2] M.M. Pendergast, E.M. Hoek, A review of water treatment membrane nanotechnologies, Energy Environ. Sci. 4 (6) (2011) 1946–1971.
[3] N. Akther, et al., Recent advancements in forward osmosis desalination: a review, Chem. Eng. J. 281 (2015) 502–522.
[4] J.-G. Gai, X.-L. Gong, Zero internal concentration polarization FO membrane: functionalized graphene, J. Mater. Chem. A 2 (2) (2014) 425–429.
[5] M. Qasim, et al., Water desalination by forward (direct) osmosis phenomenon: a comprehensive review, Desalination 374 (2015) 47–69.
[6] R.E. Kravath, J.A. Davis, Desalination of sea water by direct osmosis, Desalination 16 (2) (1975) 151–155.
[7] L. Chekli, et al., A review of draw solutes in forward osmosis process and their use in modern applications, Desalination Water Treat. 43 (1–3) (2012) 167–184.
[8] H.-g. Choi, et al., Thin-film composite membranes comprising ultrathin hydrophilic polydopamine interlayer with graphene oxide for forward osmosis, Desalination 449 (2019) 41–49.
[9] C. Tan, H. Ng, A novel hybrid forward osmosis-nanofiltration (FO-NF) process for seawater desalination: Draw solution selection and system configuration, Desalination Water Treat. 13 (1–3) (2010) 356–361.

[10] F. Perreault, A.F. De Faria, M. Elimelech, Environmental applications of graphene-based nanomaterials, Chem. Soc. Rev. 44 (16) (2015) 5861–5896.
[11] G. Liu, W. Jin, N. Xu, Graphene-based membranes, Chem. Soc. Rev. 44 (15) (2015) 5016–5030.
[12] L. Wang, et al., Sandwich layered double hydroxides with graphene oxide for enhanced water desalination. 65 (3) (2022) 803–810.
[13] M. Shan, et al., Decreased cross-linking in interfacial polymerization and heteromorphic support between nanoparticles: towards high-water and low-solute flux of hybrid forward osmosis membrane, J. Colloid Interface Sci. 548 (2019) 170–183.
[14] Z. Xu, et al., Constructing dense and hydrophilic forward osmosis membrane by cross-linking reaction of graphene quantum dots with monomers for enhanced selectivity and stability, J. Colloid Interface Sci. 589 (2021) 486–499.
[15] F. Yu, et al., High-performance forward osmosis membrane with ultra-fast water transport channel and ultra-thin polyamide layer, J. Membr. Sci. 616 (2020) 118611.
[16] Y. Yuan, et al., Enhanced desalination performance of carboxyl functionalized graphene oxide nanofiltration membranes, Desalination 405 (2017) 29–39.
[17] X. Fan, Y. Liu, X. Quan, A novel reduced graphene oxide/carbon nanotube hollow fiber membrane with high forward osmosis performance, Desalination 451 (2019) 117–124.
[18] Y. Zhang, S. Zhang, T.-S. Chung, Nanometric graphene oxide framework membranes with enhanced heavy metal removal via nanofiltration, Environ. Sci. Technol. 49 (16) (2015) 10235–10242.
[19] F. Yan, et al., Preparation of freestanding graphene-based laminar membrane for clean-water intake via forward osmosis process, RSC Adv. 7 (3) (2017) 1326–1335.
[20] E. Yang, et al., Laminar reduced graphene oxide membrane modified with silver nanoparticle-polydopamine for water/ion separation and biofouling resistance enhancement, Desalination 426 (2018) 21–31.
[21] N. Padmavathy, et al., Interlocked graphene oxide provides narrow channels for effective water desalination through forward osmosis. ACS applied materials & interfaces 11 (7) (2019) 7566–7575.
[22] P.S. Goh, et al., Recent progresses of forward osmosis membranes formulation and design for wastewater treatment, Water 11 (10) (2019) 2043.
[23] W.-S. Hung, et al., Tuning the interlayer spacing of forward osmosis membranes based on ultrathin graphene oxide to achieve desired performance, Carbon 142 (2019) 337–345.
[24] W. Wu, et al., Recent development of graphene oxide based forward osmosis membrane for water treatment: a critical review, Desalination 491 (2020) 114452.
[25] D.J. Johnson, N. Hilal, Can graphene and graphene oxide materials revolutionise desalination processes? Desalination 500 (2020) 114852.
[26] X. Wu, F. Fang, K. Zhang, Graphene oxide modified forward osmosis membranes with improved hydrophilicity and desalination performance, Desalination Water Treat. 85 (2017) 73–83.
[27] W. Xu, Q. Chen, Q. Ge, Recent advances in forward osmosis (FO) membrane: chemical modifications on membranes for FO processes, Desalination 419 (2017) 101–116.
[28] E. Yang, et al., Enhanced desalination performance of forward osmosis membranes based on reduced graphene oxide laminates coated with hydrophilic polydopamine, Carbon 117 (2017) 293–300.
[29] H. Kang, et al., Interlamination restrictive effect of carbon nanotubes for graphene oxide forward osmosis membrane via layer by layer assembly, Appl. Surf. Sci. 465 (2019) 1103–1106.
[30] J.-h. Song, et al., Tuning the nanostructure of nitrogen-doped graphene laminates for forward osmosis desalination, Nanoscale 11 (45) (2019) 22025–22032.
[31] S. Yadav, et al., Recent developments in forward osmosis membranes using carbon-based nanomaterials, Desalination 482 (2020) 114375.
[32] P. Deka, et al., Performance evaluation of reduced graphene oxide membrane doped with polystyrene sulfonic acid for forward osmosis process, Sustain. Energy Technol. Assessments 44 (2021) 101093.
[33] S. Kim, et al., Highly crosslinked, chlorine tolerant polymer network entwined graphene oxide membrane for water desalination, J. Mater. Chem. A 5 (4) (2017) 1533–1540.
[34] P.S. Parsamehr, et al., Preparation of novel cross-linked graphene oxide membrane for desalination applications using (EDC and NHS)-activated graphene oxide and PEI, Desalination 468 (2019) 114079.
[35] F. Zhao, F. Li, C.-Y. Ma, Desalination performance of graphene oxide-PEG nanohybrid membranes. 3rd Annual International Conference on Advanced Material Engineering (AME 2017), Atlantis Press, 2017.
[36] M. Niu, et al., Polyethylene glycol grafted with carboxylated graphene oxide as a novel interface modifier for polylactic acid/graphene nanocomposites, R. Soc. Open Sci. 7 (7) (2020) 192154.
[37] L.-S. Tang, et al., Polyethylene glycol/graphene oxide aerogel shape-stabilized phase change materials for photo-to-thermal energy conversion and storage via tuning the oxidation degree of graphene oxide, Energy Convers. Manag. 146 (2017) 253–264.
[38] J. Borges-Vilches, et al., Graphene oxide/polyethylene glycol aerogel reinforced with grape seed extracts as wound dressing, J. Mater. Sci. 56 (2021) 16082–16096.
[39] G.R. Plá, et al., Investigation on the morphology and the permeability of biomimetic cellulose triacetate (CTA) impregnated membranes (IM): in-situ synchrotron imaging, experimental and computational studies, Mater. Chem. Phys. 292 (2022) 126755.
[40] M. Edokali, et al., Chemical modification of reduced graphene oxide membranes: enhanced desalination performance and structural properties for forward osmosis, Chem. Eng. Res. Des. 199 (2023) 659–675.
[41] M. Edokali, et al., Antifouling and stability enhancement of electrochemically modified reduced graphene oxide membranes for water desalination by forward osmosis. Journal of Water Process Engineering 59 (2024) 104809.
[42] S. Eigler, et al., Graphene oxide: a stable carbon framework for functionalization, J. Mater. Chem. A 1 (38) (2013) 11559–11562.
[43] H. Liu, et al., In situ synthesis of the reduced graphene oxide–polyethyleneimine composite and its gas barrier properties, J. Mater. Chem. A 1 (11) (2013) 3739–3746.
[44] J. Jang, et al., Graphene oxide nanocomposite membrane cooperatively cross-linked by monomer and polymer overcoming the trade-off between flux and rejection in forward osmosis, J. Membr. Sci. 598 (2020) 117684.
[45] G. Hurwitz, G.R. Guillen, E.M. Hoek, Probing polyamide membrane surface charge, zeta potential, wettability, and hydrophilicity with contact angle measurements, J. Membr. Sci. 349 (1–2) (2010) 349–357.
[46] J.-T. Chen, et al., Tuning nanostructure of graphene oxide/polyelectrolyte LbL assemblies by controlling pH of GO suspension to fabricate transparent and super gas barrier films, Nanoscale 5 (19) (2013) 9081–9088.
[47] X. Zhou, et al., The carbonization of polyethyleneimine: facile fabrication of N-doped graphene oxide and graphene quantum dots, RSC Adv. 5 (128) (2015) 105855–105861.
[48] Z. Jia, Y. Wang, Covalently crosslinked graphene oxide membranes by esterification reactions for ions separation, J. Mater. Chem. A 3 (8) (2015) 4405–4412.
[49] R. Aghehrochaboki, et al., Polyethyleneimine functionalized graphene oxide/methyldiethanolamine nanofluid: preparation, characterization, and investigation of CO2 absorption, J. Environ. Chem. Eng. 7 (5) (2019) 103285.
[50] S. Stankovich, et al., Graphene-based composite materials, Nature 442 (7100) (2006) 282–286.
[51] C.-N. Yeh, et al., On the origin of the stability of graphene oxide membranes in water, Nat. Chem. 7 (2) (2015) 166–170.
[52] Y. Su, et al., Impermeable barrier films and protective coatings based on reduced graphene oxide, Nat. Commun. 5 (1) (2014) 4843.
[53] A.M. Díez-Pascual, A.L. Díez-Vicente, Poly (propylene fumarate)/polyethylene glycol-modified graphene oxide nanocomposites for tissue engineering, ACS Appl. Mater. Interfaces 8 (28) (2016) 17902–17914.
[54] N.D. Mao, et al., Polyethylene glycol functionalized graphene oxide and its influences on properties of Poly (lactic acid) biohybrid materials, Compos. B Eng. 161 (2019) 651–658.
[55] W. Gao, The chemistry of graphene oxide. Graphene oxide: reduction recipes, spectroscopy, applications (2015) 61–95.
[56] W. Yu, et al., Progress in the functional modification of graphene/graphene oxide: a review, RSC Adv. 10 (26) (2020) 15328–15345.
[57] S. Eigler, et al., Formation and decomposition of CO2 intercalated graphene oxide, Chem. Mater. 24 (7) (2012) 1276–1282.
[58] P.P. Brisebois, R. Izquierdo, M. Siaj, Room-Temperature reduction of graphene oxide in water by metal chloride hydrates: a cleaner approach for the preparation of graphene@ metal hybrids, Nanomaterials 10 (7) (2020) 1255.
[59] H. Wang, Y.H. Hu, Electrolyte-induced precipitation of graphene oxide in its aqueous solution, J. Colloid Interface Sci. 391 (2013) 21–27.
[60] V.D. Ebajo Jr., et al., Regenerable acidity of graphene oxide in promoting multicomponent organic synthesis, Sci. Rep. 9 (1) (2019) 15579.
[61] G. Socrates, Infrared and Raman Characteristic Group Frequencies: Tables and Charts, John Wiley & Sons, 2004.
[62] H. Liu, et al., Synthesis of polyethylenimine/graphene oxide for the adsorption of U (VI) from aqueous solution, Appl. Surf. Sci. 471 (2019) 88–95.
[63] V. Vatanpour, et al., Cellulose acetate in fabrication of polymeric membranes: a review, Chemosphere 295 (2022) 133914.
[64] M.-Y. Lim, et al., Cross-linked graphene oxide membrane having high ion selectivity and antibacterial activity prepared using tannic acid-functionalized graphene oxide and polyethyleneimine, J. Membr. Sci. 521 (2017) 1–9.
[65] F.-Y. Zhao, et al., High-flux positively charged nanocomposite nanofiltration membranes filled with poly (dopamine) modified multiwall carbon nanotubes. ACS applied materials & interfaces 8 (10) (2016) 6693–6700.
[66] S. Sahebi, et al., Thin-film composite membrane on a compacted woven backing fabric for pressure assisted osmosis, Desalination 406 (2017) 98–108.
[67] B. Yu, et al., Pdop layer exhibiting zwitterionicity: a simple electrochemical interface for governing ion permeability, Chem. Commun. 46 (32) (2010) 5900–5902.
[68] D. Li, et al., Processable aqueous dispersions of graphene nanosheets, Nat. Nanotechnol. 3 (2) (2008) 101–105.
[69] H. Liu, H. Wang, X. Zhang, Facile fabrication of freestanding ultrathin reduced graphene oxide membranes for water purification, Adv. Mater. 27 (2) (2015) 249–254.
[70] B. Li, et al., One-step electrochemically prepared graphene/polyaniline conductive filter membrane for permeation enhancement by fouling mitigation, Langmuir 36 (9) (2020) 2209–2222.
[71] M. Al-Furaiji, et al., Preparation of thin-film composite membranes supported with electrospun nanofibers for desalination by forward osmosis. Drinking Water Engineering and Science 13 (2) (2020) 51–57.
[72] M. Kadhom, B. Deng, Synthesis of high-performance thin film composite (TFC) membranes by controlling the preparation conditions: technical notes, J. Water Proc. Eng. 30 (2019) 100542.
[73] A. Ilyas, et al., Micro-patterned cellulose triacetate membranes for forward osmosis: synthesis, performance and anti-fouling behavior, Desalination 542 (2022) 116076.

[74] M.B.M.Y. Ang, et al., Merits of using cellulose triacetate as a substrate in producing thin-film composite nanofiltration polyamide membranes with ultra-high performance, J. Taiwan Inst. Chem. Eng. 112 (2020) 251–258.
[75] R.C. Ong, T.-S. Chung, Fabrication and positron annihilation spectroscopy (PAS) characterization of cellulose triacetate membranes for forward osmosis, J. Membr. Sci. 394 (2012) 230–240.
[76] T. Sunohara, T. Masuda, Cellulose triacetate as a high-performance membrane. High-performance membrane dialyzers 173 (2011) 156–163.
[77] M.D. Islam, et al., Cellulose acetate-based membrane for wastewater treatment—a state-of-the-art review, Mater. Adv. 4 (18) (2023) 4054–4102.
[78] E. Nagy, Basic Equations of Mass Transport through a Membrane Layer, Chapter 3-Mass Transport through a Membrane Layer, Elsevier, 2018, pp. 21–68.
[79] E. Langer, et al., Plasticizers Derived from Post-consumer PET: Research Trends and Potential Applications, Chapter 3-Essential Quality Parameters of Plasticizers, Applied Science Publishers, 2019, pp. 45–100.
[80] L. Huynh, et al., Computational approaches to the rational design of nanoemulsions, polymeric micelles, and dendrimers for drug delivery, Nanomed. Nanotechnol. Biol. Med. 8 (1) (2012) 20–36.
[81] D. Rana, B. Mandal, S. Bhattacharyya, Miscibility and phase diagrams of poly (phenyl acrylate) and poly (styrene-co-acrylonitrile) blends, Polymer 34 (7) (1993) 1454–1459.
[82] D. Rana, B. Mandal, S. Bhattacharyya, Analogue calorimetric studies of blends of poly (vinyl ester) s and polyacrylates, Macromolecules 29 (5) (1996) 1579–1583.
[83] V. Vatanpour, et al., Cellulose acetate in fabrication of polymeric membranes: a review, Chemosphere 295 (2022) 133914.
[84] S. Kadanyo, et al., Enhancing compatibility and hydrophilicity of polysulfone/poly (ethylene-co-vinyl alcohol) copolymer blend ultrafiltration membranes using polyethylene glycol as hydrophilic additive and compatibilizer, Separ. Purif. Technol. 287 (2022) 120523.
[85] X. Tong, et al., A freestanding graphene oxide framework membrane for forward osmosis: Separation performance and transport mechanistic insights, J. Membr. Sci. 661 (2022) 120919.